

CFD Modeling of Sodium-Oxide Deposition in Sodium-Cooled Fast Reactor Compact Heat Exchangers

E. Tatli, J. P. Mazzocchi and P. Ferroni

Westinghouse Electric Company LLC

1000 Westinghouse Drive, Cranberry Township, PA 16066, USA

tatlie@westinghouse.com, mazzocjp@westinghouse.com, ferronp@westinghouse.com

ABSTRACT

The possible use of compact heat exchangers (HXs) in sodium-cooled fast reactors (SFR) employing a Brayton cycle is promising due to their high power density and resulting small volume in comparison with conventional shell-and-tube HXs. However, the small diameter of their channels makes them more susceptible to plugging due to Na₂O deposition during accident conditions. Although cold traps are designed to reduce oxygen impurity levels in the sodium coolant, their failure, in conjunction with accidental air ingress into the sodium boundary, could result in coolant oxygen levels that are above the saturation limit in the cooler parts of the HX channels. This can result in Na₂O crystallization and the formation of solid deposits on cooled channel surfaces, limiting or even blocking coolant flow. The development of analysis tools capable of modeling the formation of these deposits in the presence of sodium flow will allow designers of SFRs to properly size the HX channels so that, in the scenario mentioned above, the reactor operator has sufficient time to detect and react to the affected HX. Until now, analytical methodologies to predict the formation of these deposits have been developed, but never implemented in a high-fidelity computational tool suited to modern reactor design techniques. This paper summarizes the challenges and the current status in the development of a Computational Fluid Dynamics (CFD) methodology to predict deposit formation, with particular emphasis on sensitivity studies on some parameters affecting deposition.

Keywords: Sodium-cooled fast reactors, compact heat exchangers, channel plugging, sodium oxide, deposit formation, Computational Fluid Dynamics (CFD)

1. INTRODUCTION

The vast majority of Sodium-cooled Fast Reactor (SFR) designs, including those actually built and operated, adopt a conventional water/steam Rankine power conversion cycle [1]. An alternative design, seriously investigated only in the last 10-15 years due to recent progress in turbomachinery and compact heat exchanger (HX) technologies, uses instead a Brayton cycle with Supercritical CO₂ (S-CO₂) as working fluid. The choice of S-CO₂ is motivated not only by safety considerations related to the elimination of sodium-water reaction in the HXs, but also by economics considerations which are important given the perceived higher capital cost of SFRs with respect to large LWRs. In addition to capital savings resulting from the reduced, albeit not eliminated, requirements for monitoring/addressing sodium leaks, the properties of S-CO₂ result in reduced compression work, which benefits plant conversion efficiency, and in remarkably small turbomachinery, especially the turbine. All these aspects

are clearly conducive to better economics. On the other hand, however, the heat transfer properties of S-CO₂ are similar to those of conventional gases, thus requiring a large heat transfer area to remove the prescribed heat duty. When combined with the high pressures (up to 20 MPa) and relatively high temperatures (up to 550 °C) characterizing an SFR-S-CO₂ plant system, this requirement results in very large, and thus expensive HXs if conventional shell-and-tube HXs were used [2]. For this reason, emphasis is recently being given to the potential use of small-channel HXs, such as diffusion-bonded HXs, since the small size of their channels result in an extreme compactness. At the same time, however, this small size also results in higher susceptibility to plugging. In the particular case of SFRs, plugging may result from sodium oxide (Na₂O) deposition, which could take place in the event of failure of the sodium boundary (and therefore air ingress) and simultaneous failure of the cold traps designed to capture impurities in the coolant. A Computational Fluid Dynamics (CFD) analysis tool capable of modeling the formation of Na₂O deposits, as well as sodium flow in presence of these deposits, will aid SFR designers to properly size the HX channels accounting for deposition/plugging considerations, and allowing the reactor operator sufficient time to detect and react to the affected HX before complete channel plugging occurs. Development and validation of these tools is the ultimate objective of the U.S. DOE sponsored research [3] carried out jointly by Westinghouse and Argonne National Laboratory (ANL). The challenges and the current status of the CFD modeling development are summarized in the following sections. Specifically:

- Section 2 discusses the motivation and objective of the work, and briefly describes deposition models and the experimental facility used to support the project
- Section 3 explains the analysis methodology
- Section 4 presents preliminary modeling results
- Section 5 presents conclusions and summarizes future work

2. BACKGROUND

The main objective of the project is to ultimately develop properly validated CFD models able to predict Na₂O deposition in small-diameter channels, and thus the time for their complete plugging. Integral part of this effort is the use of the Sodium Plugging Phenomena Loop (SPPL), operated by ANL, which will be used to support the validation effort, as well as to gain insights on the Na₂O deposit growth [4]. In particular, because of the impossibility to open the facility to examine the deposits without perturbing them (due to the air-induced oxidation), ANL is developing diagnostic, non-invasive techniques to identify deposition locations and possibly to characterize the deposits. These efforts, which are part of the project, are not however discussed in this paper, but might be used to validate the CFD models under development.

When liquid sodium contains dissolved oxygen and it is cooled below the saturation temperature for oxygen dissolution [5, 6], Na₂O tends to nucleate and grow on the surfaces that are cooled, leading to formation of solid deposits. An analytical approach to these phenomena has recently been reported by Sienicki in the context of a phenomenological model of deposit growth, based upon oxygen mass transfer between the sodium and the deposit ([4], [7]). Although this model represents an improvement with respect to previous investigations due to the introduction of the concept of deposit porosity, it does not capture in full detail the heat transfer (between the fluid and the wall/deposit) nor the fluid dynamics effects locally, and it is not available within a state-of-the-art computational framework suited for coupling to modern reactor design/analysis tools. The work described herein presents the current status of an effort aimed at extending this treatment and addressing its limitations through the development of a validated CFD model that predicts local deposition based on modeling of the temperature-dependent growth characteristics of Na₂O.

2.1 Brief Survey of Available Analytical Models for Sodium Oxide Deposition

Based on recent reported work, two models were considered for the deposition of Na_2O for this particular project [8]: the first principles model by Sienicki [7] and a mass-transfer kinetics model by Khatcheressian et al. [10]. The first principles model calculates a 1-D linear growth of a two-phase deposit consisting of liquid sodium and solid Na_2O volume fractions within a HX channel of a given shape. The growth of this deposit is a function of an overall mass transfer coefficient defined by local dimensionless heat or mass transfer numbers, the oxygen concentration gradient between the surface of the deposit (or the HX wall), the equilibrium oxygen concentration in the system, and the effective oxygen density in the deposit [7]. Localized Nusselt numbers can be used to describe the oxygen mass transfer process for either turbulent or laminar forced flow convection using the mass and heat transfer analogy [7, 9]. After review it was concluded that this model provides a flexible mathematical approach for calculating deposit growth and is also advantageous since it had been compared against a plugging experiment at the SPPL under laminar flow, predicting the time of growth of a deposit within $\sim 25\%$ of a measured value [7].

The mass-transfer kinetics model predicts instead the growth of Na_2O and sodium hydride (NaH) deposits in larger scale cold traps that contain packing [10]. In addition to mass-transfer considerations, this model also incorporates rate constants associated with both crystal nucleation and growth. The model provides the potential for a more fundamental description of the crystallization process; however kinetic parameters were not well defined for the HX channel conditions relevant to this project and values needed for the calculation of the kinetic parameters were also reported as confidential [11]. For these reasons, early modeling efforts are focusing on the use of the first principles model [7] with the CFD analysis. Certain aspects of the mass-transfer kinetics model may be incorporated in future efforts.

2.2 ANL SPPL Facility Description

The SPPL facility at ANL will be used to collect Na_2O deposition data in order to benchmark corresponding CFD models. The facility consists of a sodium loop in which Na_2O deposition is induced inside test sections each containing sets of small-diameter (2, 4 and 6 mm in its original setup) semi-circular channels, by adding Na_2O granules to the flow and reducing the test section temperature below the oxygen solubility value. The original setup of the loop is shown in Figure 1, and the loop is currently being upgraded, reducing the three test sections to only one, containing three 6 mm semi-circular channels. More information on the facility and its operation can be found in [12].

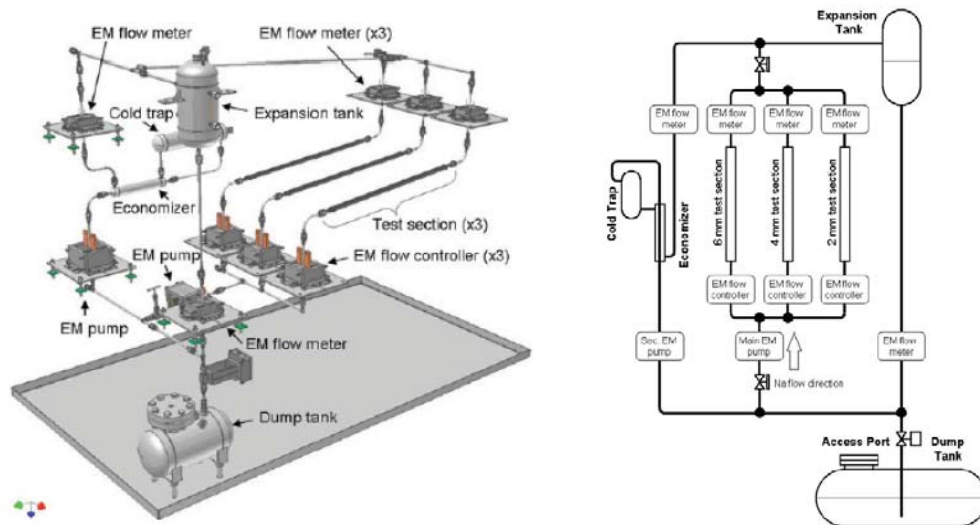


Figure 1: ANL Sodium Plugging Phenomena Loop (SPPL), original setup [12]

3. ANALYSIS METHODOLOGY

3.1 Operating Conditions

The CFD modeling approach will be focused mainly on reproducing (and validating with) the flow rate, pressure drop and temperature measurements from the SPPL. Thus, in addition to the inherent uncertainties in deposit properties due to lack of available data, the CFD modeling approach needs to be tested across all the flow rates and temperatures (inlet and cooling) that can be simulated with the facility, and should also assess geometric parameters that can affect fluid dynamics and deposition (entry path to the test channels, cooled section lengths, etc.).

Based on the flow rate versus temperature calibration curve for the original SPPL 6 mm semi-circular test section presented in [12], conservative lower and upper Reynolds numbers of approximately 100 and 1500 were used in the CFD analysis. In addition, based on the temperatures given in [13], the sodium inlet temperature considered for the model presented herein was chosen to be 300 °C, and the cooled section surface temperature was set to 150 °C. These values may change depending on future use and setup of the SPPL, and are used here as a starting point.

3.2 Sodium and Sodium Oxide (Na₂O) Properties

In the current CFD model, sodium density, dynamic viscosity, thermal conductivity and specific heat are used as a function of temperature and are taken from [14].

Unlike for pure sodium, for Na₂O and for Na-Na₂O mixtures, data on deposit structure and thermo-physical properties are scarce. The following subsections discuss how the properties for Na₂O are computed. Multiple approaches are instead used to estimate properties for Na-Na₂O mixtures, as discussed in Section 3.4.

Density

The solid oxide volume fraction of the deposit was assumed to have a temperature-independent density equivalent to the theoretical density of 2270 kg/m³ [15].

Specific heat

Specific heat data are available in literature for solid sodium oxide [16, 17].

$$\text{Specific heat } \left(\frac{J}{kgK}\right) = -0.0013568 * [T(K)]^2 + 2.1272 * T(K) + 593.02 \quad (1)$$

Thermal conductivity

Estimating the thermal conductivity of the solid phase Na₂O portion of the deposit as a function of temperature is necessary to thoroughly consider heat transfer effects within the plugging of HX channels. A literature search provided no direct data for the thermal conductivity of pure Na₂O [18 - 21], and little thermal conductivity data was found for oxides of similar composition materials such as pure Li₂O or K₂O. However, thermal conductivity data for solid Na₂O-sodium cermets was available at a single temperature of 55 °C [18, 19] as a function of Na₂O composition (5-60 wt %). The thermal conductivity data for solid sodium is also available at temperatures below the sodium melting point of 97.72 °C [14, 18].

Using this data, the thermal conductivity of pure Na₂O at 55 °C was calculated using relationships provided by [22] that estimate the thermal conductivity of mixed solid materials. In this approach, it was assumed that the structure of the cermet could be described using a cubic geometry, in which Na₂O is the continuous phase and sodium is the discrete phase. Since the thermal conductivity of the Na₂O-sodium cermet and its solid sodium fraction were known at 55 °C from the literature, it was possible to back calculate the thermal conductivity of the Na₂O fraction using an effective thermal conductivity relationship that is composition dependent [22]. A thermal conductivity value for the Na₂O fraction of the cermet was calculated for each cermet composition reported in [18] and [19], and the values were averaged. The resulting thermal conductivity value for solid Na₂O was equal to 9.5 W/m.K (± 42%). While the intrinsic value of the Na₂O thermal conductivity should be independent of the cermet composition (recognizing the overall cermet thermal conductivity will be a function of specific sodium and Na₂O compositions), this method provided a preliminary estimate of Na₂O conductivity at a single temperature of 55 °C.

However, the temperature in the HX channel will typically be above the melting point of sodium (i.e. > ~ 98.0 °C), and therefore the Na₂O thermal conductivity value calculated at 55 °C was scaled to higher temperatures using the thermal conductivity behavior of MgO at temperatures between 27 °C and 277 °C [23] (MgO is the closest material with available data). A polynomial regression for MgO thermal conductivity as a function of temperature was plotted. A “base” thermal conductivity of 56.2 W/m.K was extrapolated for MgO at 55 °C. The percentage change in MgO thermal conductivity from this base value to higher temperatures was then used to scale the Na₂O thermal conductivity of 9.5 W/m.K for the same temperature change. Using this approach, a temperature dependent curve for the thermal conductivity of Na₂O was extrapolated between 150 °C and 300 °C as shown in Equation 2 (thermal conductivity decreases from ~ 6.5 W/m.K to ~ 4 W/m.K, from 150 °C to 300 °C, respectively).

$$\text{Thermal conductivity } \left(\frac{W}{m \cdot K}\right) = -2.519e - 7 * [T(K)]^3 + 3.91e - 4 * [T(K)]^2 - 0.2176 * T(K) + 47.66 \quad (2)$$

3.3 Preliminary Modeling Approach

The formation of the deposit on the walls is first and foremost driven by the local temperature and oxygen concentration. In order to reduce the number of variables in this preliminary phase of the modeling the oxide deposit formation was assumed to be directly linked to the local temperature instead of first determining the deposit mass flux due to temperature-dependent oxygen solubility and concentration (which will be included in future work). A simple relationship was assumed between liquid sodium volume fraction and temperature, based on a 150 °C cooled wall set up in the original SPPL [13] in which sodium volume fraction was set to 0, and a linear rise to a value of 1 at 160 °C. This means that between temperatures of 150 °C and 160 °C there is a mixture of sodium and Na₂O, and at any temperature at or above 160 °C only liquid sodium exists. This simplified assumption, in this preliminary stage, will be replaced by the calculated deposit mass flux based on local temperature, oxygen concentration and solubility of oxygen in liquid sodium ([4, 5]) such as presented in [8].

ANSYS CFX v14.5.7 [24] (CFX) was used as pre-processor, solver, and post-processor for the CFD work presented herein. In order to simulate the deposit formation, the multi-component fluid structure of CFX was utilized [24, 25]. Within this analysis, two materials co-exist – namely liquid sodium and the deposit, and depending on the temperature observed on the computational cell, a combination of these materials are present. In this preliminary approach, the local temperature was used to determine the liquid sodium volume fraction based on the relationship explained above, as a simplified assumption. In order to

account for the loss of momentum due to the solidification process, momentum sinks were placed on each cell with a mass fraction of sodium less than 0.8, an assumed value for the preliminary analysis. Turbulence and energy sinks were not added at this stage, but will be incorporated in future models. Sinks added in the future will be functions of local solidification fractions.

3.4 Test Matrix

A sensitivity study was conducted on some of the many parameters expected to affect deposit formation. These parameters are briefly discussed below and summarized in Table 1 which shows the complete test matrix considered in the work presented herein.

- Reynolds number: As mentioned before, Re values from approximately 100 to 1500 were tested in the 6 mm diameter semi-circular channels in the original SPPL [12]. These two values are considered for the analysis herein as bounding values.
- Deposit thermal conductivity: No direct data for pure Na₂O thermal conductivity is available in the literature, nor the composition/structure of the deposit is known. As expected, the thermal conductivity of the deposit will have an important impact on deposit formation, and thus a sensitivity analysis with two sets of deposit thermal conductivity values with respect to temperature were tested.
 1. Deposit thermal conductivity is assumed to be equal to that of “pure” Na₂O derived in Section 3.2, Equation 2, i.e. without sodium inside the deposit.
 2. Considering the deposit solid fraction value of 0.18 from Sienicki [7], an ‘effective’ deposit thermal conductivity was calculated as a function of temperature, using Equation 3 (thermal conductivity decreases from ~ 71 W/m.K to ~ 63 W/m.K, from 150 °C to 300 °C, respectively).

$$\text{‘Effective’ deposit thermal conductivity } \left(\frac{W}{mK}\right) = k_{Na_2O}(T) * (0.18) + k_{Sodium}(T) * 0.82 \quad (3)$$

- Cooled section length: Two cooled section lengths of 6 mm (L/D = 1) and 12 mm (L/D = 2) were used to study the effects on deposit formation.

Table 1: Test matrix

Case #	Re	Deposit Thermal Conductivity	Cooled Section Length (mm)
1	100	Na ₂ O	6
2	1500	Na ₂ O	6
3	100	Effective	6
4	1500	Effective	6
5	100	Na ₂ O	12
6	1500	Na ₂ O	12
7	100	Effective	12
8	1500	Effective	12

3.5 CFD Model

In the process of developing the preliminary numerical modeling approach of the deposit final shape formation, prior to modeling the full SPPL in 3-D, a 2-D model representative of one of the 6 mm diameter semi-circular test channels was built. A 6 mm wide 2-D domain (two computational cells thick), with an entrance section, a cooled section, and an exit section was built, as shown in Figure 2. The entrance section length was 240 mm ($L/D = 40$), and exit section length was 60 mm ($L/D = 10$), both lengths representative of the dimensions in the SPPL.

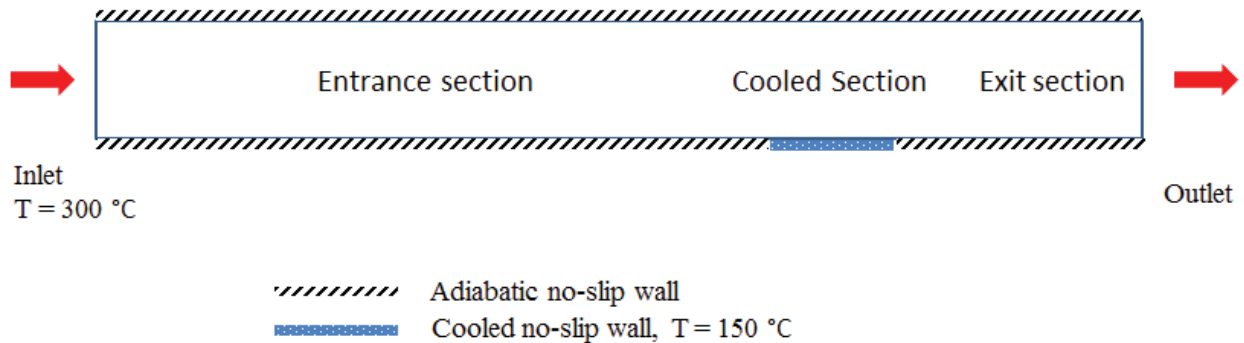


Figure 2: 2-D CFD domain (not to scale)

This domain was meshed using TrueGrid [26] with hexahedral cells. The total number of cells for the 6 mm cooled section model was 282,720, and it was 297,600 for the 12 mm cooled section model. A cut plane showing mesh density near the lower wall is presented in Figure 3.

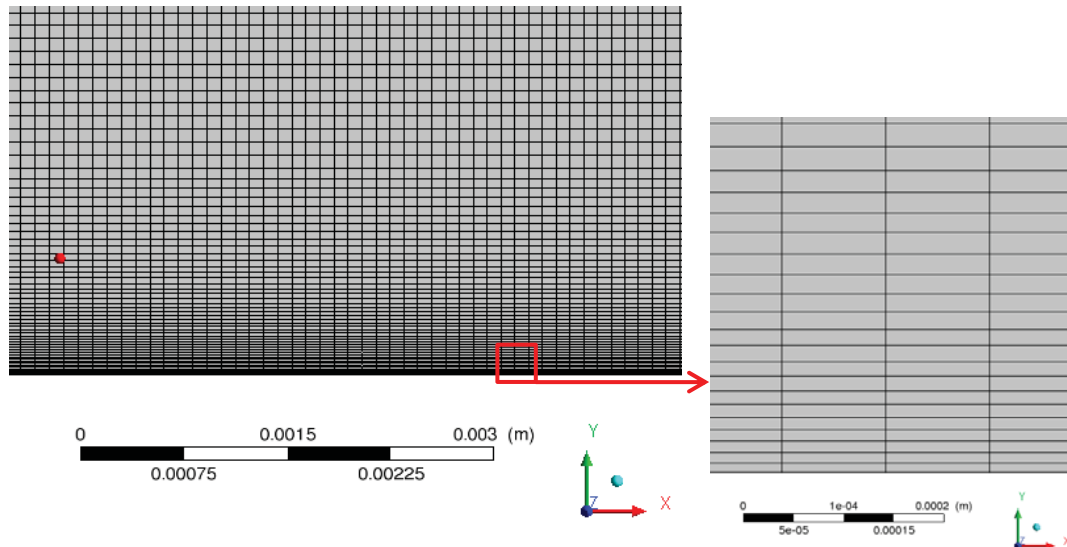


Figure 3: Cut plane showing mesh density on the lower wall (first layer thickness = 0.01 mm)

Uniform velocity profiles were prescribed for the inlet at values of 0.006468 m/s and 0.097027 m/s at 300 °C, corresponding to Re values of 100 and 1500, respectively. SST $k-\omega$ turbulence model [27] with

automatic wall function was prescribed for both Re values, with a turbulent Prandtl number (Pr_t) of 4.12¹ [28-30]. Note that although the Re values technically fall under laminar regime (as discussed in the results section), the formation of deposits may cause narrowing of the channel and recirculation regions behind the deposit, and thus need to be accounted for as these effects may have a strong influence on the flow regime transition and deposit formation. Thus, the sensitivity studies and comparison of the laminar versus turbulent flow model results were performed. A 1% inlet turbulence intensity was prescribed for the analyses presented herein, but sensitivity studies on this value will be conducted in the future to account for possible upstream effects in the SPPL.

At the exit of the domain, an opening boundary condition in CFX was applied (which allows recirculation at the exit), with 0 psi gage pressure and 300 °C temperature. Authors determined this to be a critical decision over choosing an outlet boundary condition (which blocks the recirculation inflows during the calculation) with respect to providing run stability. The choice for opening boundary condition provides all outlet velocities (no recirculation) at the end of the calculation when the run converges as there is no back flow 60 mm ($L/D = 10$) downstream of the cooled section for any of the cases presented herein.

Symmetry boundary conditions were applied at the two computational cells thick domain outer vertical sides. All walls were prescribed no-slip boundary conditions and all walls except the cooled wall were chosen to be adiabatic.

All cases were run as steady state, using double precision. The domain imbalances were monitored for convergence as well as monitoring points for sodium mass fraction, temperature, and velocities placed throughout the domain. The time steps (pseudo time steps in CFX steady state simulations, acting as under-relaxation factors) required for stable runs were determined to be very small (as low as in the order of 1.e-5 seconds) resulting in long run times until the final steady state deposit shape is reached. Each case was run until total pseudo time had reached at least two full residence times. The final models will be run in transient mode to evaluate the time-dependent nature of the deposit formation and validate against time-varying experimental data from SPPL when available (such as test section pressure drop).

4. RESULTS

Results are shown below starting with the effect of the test matrix parameters on the sodium mass fraction for the eight cases, followed by a more detailed discussion on one case only, i.e. Case 5.

Figure 4 shows the sodium mass fraction contour plots on the center cut plane for Cases 1 through 4 (6 mm cooled section). It can be observed that:

- Re number has a strong effect on the deposit shape. This is an expected phenomenon as the flow velocity over the cooled section (and any deposit) increases, the convective heat transfer is also enhanced, thus the opportunity of the deposit to grow is reduced by the sodium flow effectively heating the area around the cooled section.
- The thermal conductivity of the deposit has also an effect on the deposition, especially at low Re. The ‘effective’ deposit thermal conductivity is approximately 12 times higher than the thermal conductivity for ‘pure’ Na_2O (derived as explained in Section 3.2) in the temperature range between 150 °C and 300 °C. With the increase in the thermal conductivity of the deposit, conduction through

¹ Sensitivity studies conducted for [28] on Pr_t showed that results do not significantly vary between 0.9 (CFX default), 4.12 ([29]), and 5.6 ([30]) for the domain and conditions of interest in this project.

the deposit is enhanced, thus reducing the temperature of the flow around the cooled section more effectively, and thus growing the deposit deeper into the channel through solidification.

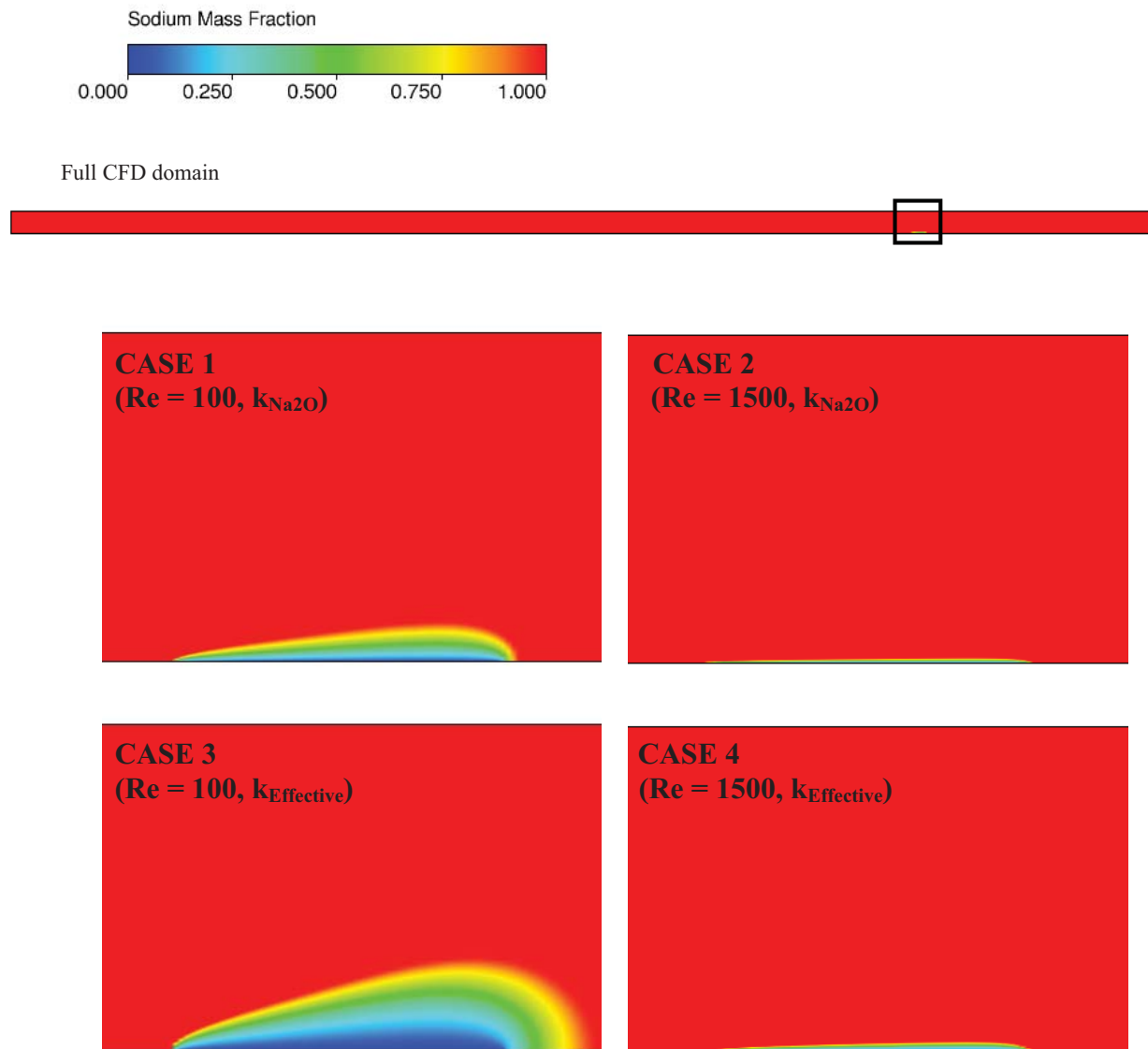


Figure 4: Sodium mass fraction contour plots for Cases 1 through 4 (cooled section length = 6 mm), zoomed in on the cooled section within the black box marked on the full CFD domain.

Figure 5 shows the sodium mass fraction contour plots on the center cut plane for Cases 5 through 8 (12 mm cooled section). The same observations can be made as for Cases 1 through 4 regarding the effect of Re and deposit thermal conductivity. In addition, comparing Cases 1 through 4 to Cases 5 through 8, one can observe that doubling the length of the cooled section had significantly expanded the deposit shape for cases with lower Re numbers, as expected. In particular, for Case 7, noting that momentum sinks are implemented on any cell with sodium mass fraction of less than 0.8, one can observe that the channel is

completely blocked by the deposit formation and that there is no more flow through the channel. The heat transfer through the rest of the downstream channel is through pure conduction.

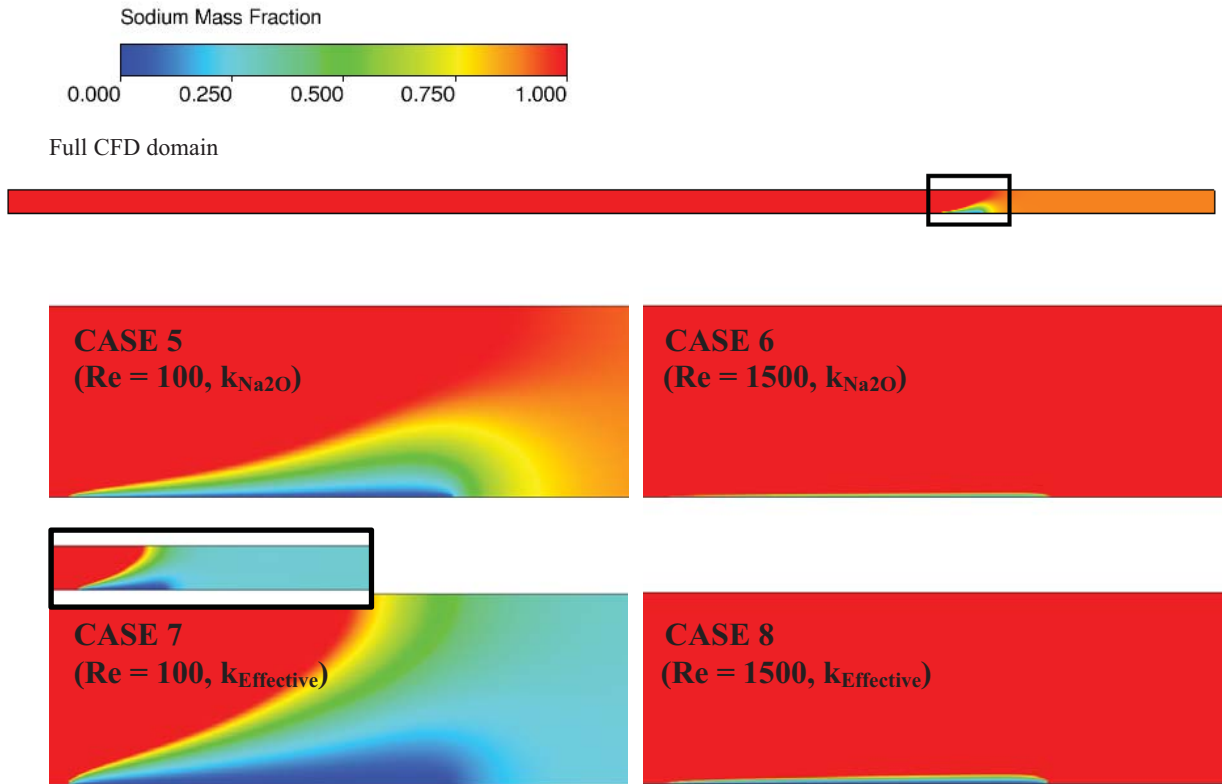


Figure 5: Sodium mass fraction contour plots for Cases 5 through 8 (cooled section length = 12 mm), zoomed in on the cooled section within the black box marked on the full CFD domain (inset for Case 7 shows the sodium mass fraction values further downstream).

Figure 6 shows the temperature contour plot for Case 7 around the cooled section vicinity (similar to Figure 5, Case 7 inset). Note that a mixture of sodium and deposit is observed between 150 °C and 160 °C, and at any temperature higher than 160 °C, only sodium is observed.

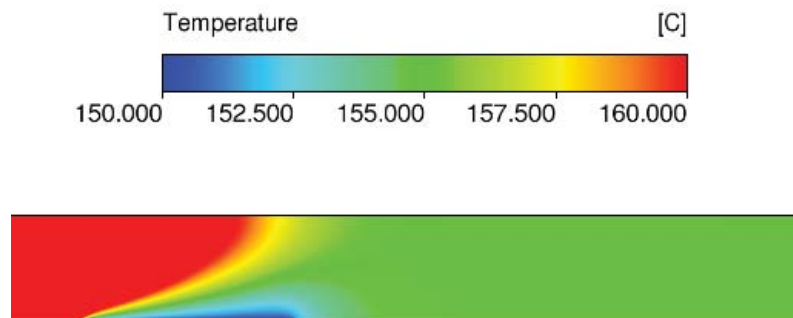


Figure 6: Temperature contour plot on vertical cut plane for Case 7 around the cooled section vicinity

More detailed results are now presented for Case 5.

The SST $k-\omega$ turbulence model was used for all the cases regardless of Re values and possible flow regime changes due to the channel narrowing and possible recirculation zones downstream of the deposits. To evaluate applicability of turbulence modeling for low Re number (in fact laminar flow) cases, Case 5 was run with both SST $k-\omega$ turbulence model (referred to as Case 5) and with no turbulence model (Laminar – referred to as Case 5-Laminar). Figure 7 shows the contour plots of sodium mass fraction around the cooled wall, showing no significant difference.

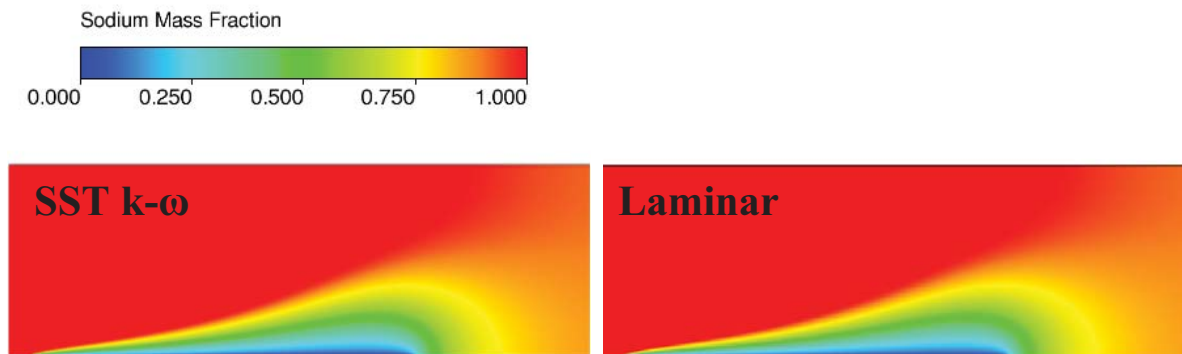


Figure 7: Comparison of sodium mass fraction contour plots on center vertical cut plane near the cooled wall for Case 5 turbulent and laminar models

Figure 8 presents the comparison of sodium mass fraction values for Case 5 turbulent and laminar models across a line perpendicular to flow (shown in black in figure inset) at a distance of 251 mm from the inlet (cooled section extends from 240 mm to 252 mm). It can be noticed that the difference between the curves is negligible.

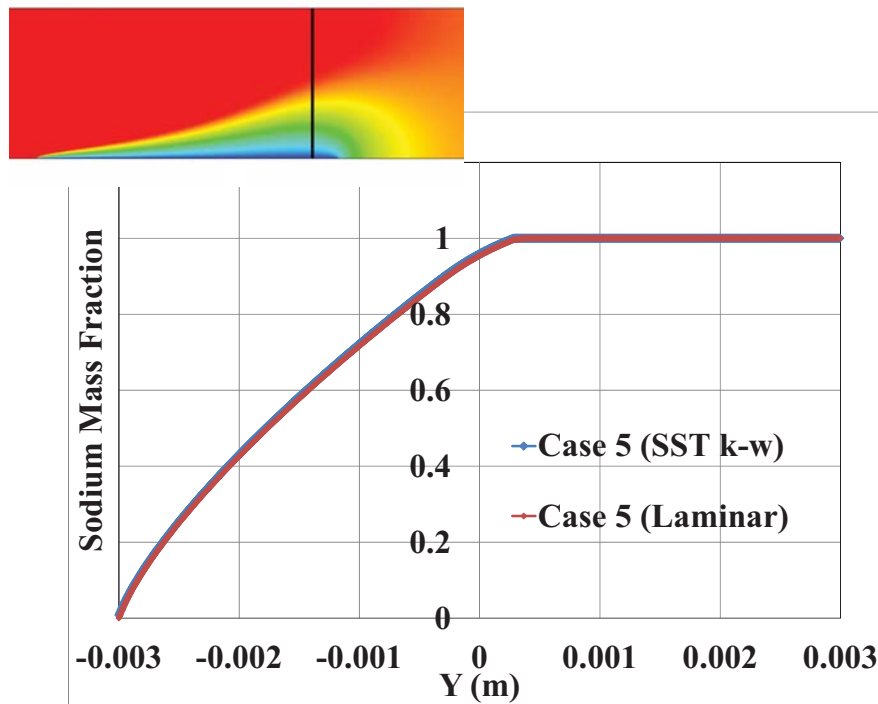


Figure 8: Comparison of sodium mass fraction values at X = 251 mm along the black line shown in insert contour plot (Y = 0 mm is the channel centerline) for Case 5 turbulent and laminar models

Figure 9 presents the temperature contour plot along the domain for Case 5. Due to the low flow rates and high thermal conductivity of sodium, sodium upstream of the cooled surface is also cooled down through conduction.

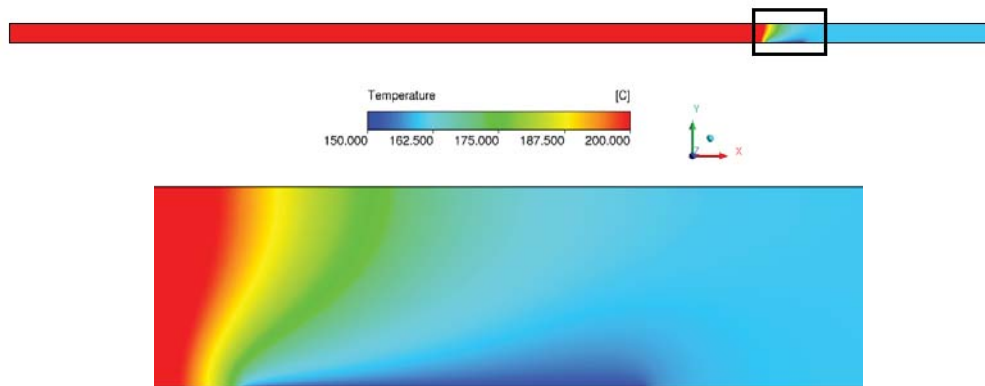


Figure 9: Temperature contour plot for Case 5, zoomed in on the cooled section

Figure 10 presents the velocity contour plots and streamlines for Case 5 and the change in the flow structure due to the deposit presence. As mentioned previously, although low Re numbers are reported in the channel, one can observe the recirculation region behind the deposit as depicted by the streamline plot in Figure 10(b).

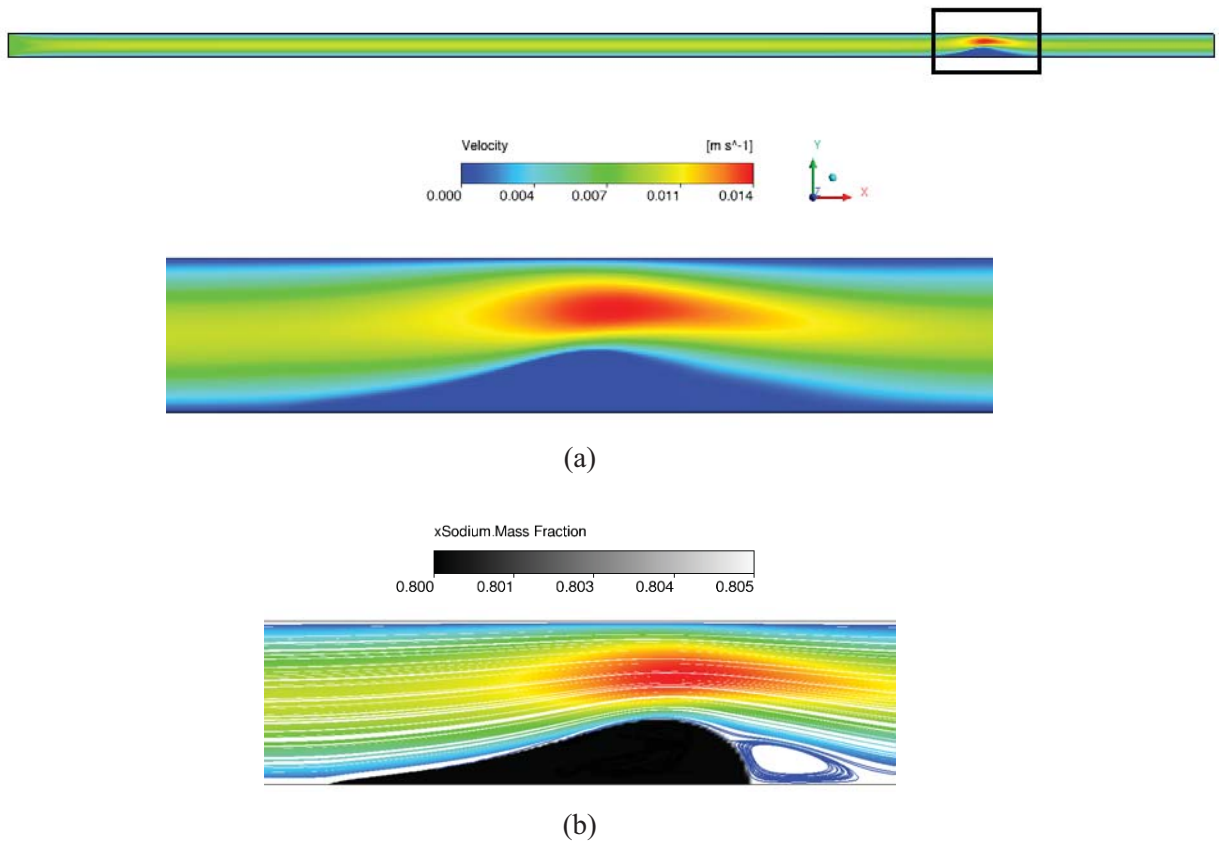


Figure 10: Velocity contour plots and streamlines for Case 5 (a) velocity magnitude contour plot around the cooled section, (b) combined sodium mass fraction contour plot and streamline velocity plot around the deposit showing the recirculation region behind the deposit (same velocity scale as in (a))

5. CONCLUSIONS AND FUTURE WORK

This paper presents the current status of CFD modeling of sodium plugging for heat exchangers in sodium-cooled fast reactor systems and several sensitivity studies on the sodium oxide deposit final shape and resulting flow and temperature fields. CFD modeling has been conducted to assess the effect of some key parameters, such as Reynolds number, deposit thermal conductivity and cooled section length, on the extent of Na₂O deposition. Although still assuming a simplified dependence between local temperature and deposit formation, the study revealed a strong effect of Re, which was expected, but especially a non-negligible effect played by the thermal conductivity of the deposit, which is a very unknown parameter due the lack of data on both pure Na₂O and on Na-Na₂O mixtures. The cooled section length also plays a large role in the deposit shape especially in low Re number flows (to the extent of complete plugging). The modeling approach will be refined as the project moves forward, and validated as the experimental data from SPPL become available. Future work may include:

- Inclusion of the concentration equation governing Na₂O deposition and application of possibly a combination of available analytical deposition models in literature [7, 10]
- Improvement of the current approach with modification of the sinks (momentum, turbulence, and energy) based on porosity and permeability, such as Carman-Kozeny model for possible flow through the deposit [31]
- Sensitivity studies on material/deposit properties
- Sensitivity studies on the turbulence inlet and modeling parameters
- Full 3-D SPPL modeling
- Conjugate heat transfer modeling, capturing the effects of test section walls
- Inclusion of test section slope (as observed in the SPPL test section) and gravity/buoyancy
- Consideration of magnetic effects due to the magnetic flow meters and controllers used in the SPPL

ACKNOWLEDGEMENTS

The authors would like to acknowledge the support and advice provided by Argonne National Laboratory.

This material is based upon work supported by the Department of Energy, Office of Nuclear Energy, under Award Number DE-NE0000611.

REFERENCES

1. IAEA-TECDOC-1531, Fast Reactor Database, December 2006 Update (2006).
2. A. Moisseytsev, J.J. Sienicki, "Supercritical Carbon Dioxide Brayton Cycle for SFR Applications: Optimization, Transient Analysis, and Control," International Conference on Fast Reactors and Related Fuel Cycles: Safe Technologies and Sustainable Scenarios, IAEA-CN-199/180, Paris, France, March 4-7, 2013 (2013).
3. P. Ferroni, J.J. Sienicki, "Modeling and validation of sodium plugging for heat exchangers in sodium-cooled fast reactor systems," Westinghouse internal presentation WAAP-8730, Panel on Department of Energy Investments in Advanced Nuclear Power, American Nuclear Society Winter Meeting, Washington D.C., USA, November 13, 2013 (2013).
4. J.J. Sienicki, "Modeling Sodium Oxide Deposit Growth and Sodium Plugging," International Conference on Fast Reactors and Related Fuel Cycles: Safe Technologies and Sustainable Scenarios, IAEA-CN-199/181, Paris, France, March 4-7, 2013 (2013).

5. J.D. Noden, "A General Equation for the Solubility of Oxygen in Liquid Sodium," *Journal of the British Nuclear Energy Society*, Vol. 12(1), pp. 57-62 (1973).
6. D.L. Smith, "Monitoring and Measurement of Oxygen Concentrations in Liquid Sodium," *Proceedings of the International Conference on Liquid Metal Technology in Energy Production*, Champion, PA, May 3-6, 1976 (1976).
7. J.J. Sienicki, "Unified analysis of Na₂O deposit growth and sodium plugging," *American Nuclear Society Winter Meeting*, San Diego, CA, USA, November 24, 2012 (2012).
8. J. Mazzocoli, E. Tatli, "Evaluation of liquid sodium impurity deposition models for sodium-cooled fast reactor heat exchangers," *American Institute of Chemical Engineers Annual Meeting*, Atlanta, GA, USA, November 16, 2014 (2014).
9. J.R. Welty, C.E. Wicks, R.E. Wilson, G. Rorrer, "Fundamentals of Momentum, Heat, and Mass Transfer 4th Edition," *John Wiley & Sons, Inc.*, New York, NY, pp. 552-554 (2001).
10. N. Khatcheressian, C. Latge, X. Joulia, T. Gilardi, X. Meyer "Modeling of cold traps for sodium purification in fast reactor," in *Proceedings of the 22nd European Symposium on Computer Aided Process Engineering*, June 17-20, 2012, London, Lockhardt Bogle, I.D, Fairweather, M., ed. Oxford, UK, Elsevier (2012).
11. N. Khatcheressian, "Développement d'un modèle de transferts couplés pour l'aide à la conception et à la conduite des systèmes de purification du sodium des réacteurs à neutrons rapides" Ph.D. Dissertation., L'Université de Toulouse (2013).
12. Y. Momozaki, D.H. Cho, J.J. Sienicki, A. Moiseyev, "Experimental Investigations on Sodium Plugging in Narrow Flow Channels," *Nuclear Technology*, 171, No. 2, pp. 153-160 (2010).
13. Y. Momozaki, D. Chojnowski, J. Sienicki, D. Cho, "Initial Investigation of Sodium Plugging under Unvarying Temperature Conditions Using the Upgraded Sodium Plugging Loop," *Nuclear Engineering Division, Argonne National Laboratory Report, ANL-ARC-220* (2011).
14. V. Sobolev, "Database of Thermophysical Properties of Liquid Metal Coolants for GEN-IV," *Scientific Report of the Belgian Nuclear Research Centre, SCK-CEN-BLG-1069* (2011).
15. J.A. Dean, "Lange's Handbook of Chemistry, 12th Edition", *McGraw-Hill Book Company*, New York, NY, p. 112 (1979).
16. R.T. Grimley, J.L. Margrave, "The high temperature heat content of sodium oxide," *Journal of Physical Chemistry*, Vol. 64, pp. 1763-764 (1960).
17. M.W. Chase, "Monograph 9, NIST-JANAF Thermochemical Tables Fourth Edition Part II, Cr-Zr", *Published by the American Physical Society and American Institute of Physics for NIST*, Gaithersburg, VA, p. 1648 (1998).
18. Y.S. Touloukian, R.W. Powel, C.Y. Ho, P.G. Klemens, "Thermophysical Properties of Matter Vol. 1: Thermal Conductivity of Metallic Elements and Alloys," *IFI/Plenum*, New York, NY (1970).
19. Y.S. Touloukian, R.W. Powel, C.Y. Ho, P.G. Klemens, "Thermophysical Properties of Matter Vol. 2: Thermal Conductivity of Nonmetallic Solids," *IFI/Plenum*, New York, NY (1970).
20. V.I. Subbotin, F.A. Kozlov, N.N. Ivanovskii, "Heat Transfer to Sodium under Conditions of Free and Forced Convection and when Oxides are Deposited on the Transfer Surface," *High Temperature*, Vol. 1, pp. 368-372 (1963).
21. F.A. Kozolov, I.N. Antonov, "Relation between Thermal Conductivity and Oxide Concentration in Sodium", *Atomic Energy*, Vol. 19(4), pp. 1333-1334 (1965).
22. Z. Yinping, L. Xingang, "Numerical analysis of the effective thermal conductivity of mixed solid materials", *Materials and Design*, Vol. 16 (2), pp. 91-95 (1995).

23. S. Caniglia, G.L. Barna, "Handbook of Industrial Refractories Technology – Principles, Types, Properties and Applications", Noyes Publishing, Westwood, NJ, p. 374 (1992).
24. ANSYS CFX v.14.5.7 ANSYS, Inc., www.ansys.com (2012).
25. K. Svihla, Personal Communication with E. Tatli, May, 2014 (2014).
26. TrueGrid v.2.3.2, XYZ Scientific Applications, Inc., www.truegrid.com (2009).
27. R. Thiele, W. Ma and H. Anglart, "Investigation of the Influence of Turbulence Models on the Prediction of Heat Transfer to Low Prandtl Number Fluids," The 14th International Topical Meeting on Nuclear Reactor Thermal-hydraulics, Toronto, Ontario, Canada, September 25-30, 2011 (2011).
28. E. Tatli, M.B. Dzodzo, P. Ferroni, "CFD Modeling of Heat and Mass Transfer in Heat Exchangers of Sodium-Cooled Fast Reactor Systems," ANS Winter Meeting, Anaheim, CA, USA, November 9-13, 2014 (2014).
29. X. Cheng, N. Tak, "Investigation on Turbulent Heat Transfer to Lead-Bismuth Eutectic Flows in Circular Tubes for Nuclear Applications," Nucl. Eng. Des. 236, 385–393 (2006).
30. J.D. Jackson, B.P. Axcell, A. Walton, "Mixed Convection Heat Transfer to Sodium in a Vertical Pipe," Exp. Heat Transfer, 7, pp. 71-90 (1994).
31. P. Bousquet-Melou, B. Goyeau, M. Quintard, F. Ficho, D. Gobin, "Average momentum equation for interdendritic flow in a solidifying columnar mushy zone," International Journal of Heat and Mass Transfer 45, 3651–3665 (2002).